JOURNAL OF PROPULSION AND POWER
Vol. 9, No. 1, Jan.–Feb. 1993

Dispersion of Solid Particles in Compressible Mixing Layers

Diana D. Glawe* and Mo Samimy†
Ohio State University, Columbus, Ohio 43210

Flow visualization and subsequent digital image processing were used to investigate the dispersion of solid particles in compressible free shear layers with convective Mach numbers of 0.51 and 0.86. A sheet of light formed using a Nd:YAG pulsed laser was used to illuminate the dispersed particles of nominal diameters 5, 17, and 62 μm. An intensified CCD camera captured images of the flowfield and subsequent digital image processing was used to locate particles in the images. Visual and statistical results for the $M_c = 0.51$ case showed dispersion trends similar to those in incompressible cases where particle dispersion depends largely on the ratio of particle time scale to fluid time scale (Stokes number). In particular, high levels of dispersion occurred for a range of Stokes numbers. However, results showed that three-dimensionality and disorganization of large scale structures in the higher compressibility case ($M_c = 0.86$) drastically reduced their entrainment and dispersion capabilities. Selective dispersion of particles was not observed for the range of Stokes numbers studied in the $M_c = 0.86$ case.

Nomenclature

d_p = particle diameter
M = Mach number
M_c = convective Mach number
$Re_{\theta 1}$ = Reynolds number based on θ_1
St = Stokes number
St_δ = dimensional Stokes number; $\delta \times St$
U = streamwise mean flow velocity
U_c = convective velocity
U_1 = supersonic freestream velocity
U_2 = subsonic freestream velocity
x = streamwise location; $x = 0$ at the splitter plate edge
y = vertical location; $y = 0$ at the splitter plate level
ΔU = $U_1 - U_2$
δ = flow length scale
θ_1 = incoming supersonic stream momentum thickness
μ = absolute fluid viscosity
ρ_f = fluid density
ρ_p = particle material density
τ_f = flow time scale
τ_p = particle time scale

Introduction

ONE predominant obstacle to developing an air breathing hypersonic flight vehicle is the requirement to efficiently mix fuel with a turbulent supersonic airflow.[1] Gaseous, liquid, and solid fuels are all being considered. The dispersion of liquid and solid fuel is a controlling factor in determining the stability and efficiency of a combustion system.[2,3] Emerging theoretical and experimental results are being used to identify the key variables that enhance or suppress particle dispersion. This knowledge is particularly important in the wake of findings that the compressibility significantly reduces the mixing growth rate[4,5] and the turbulence level and the turbulent momentum exchange.[6,7] In the project reported in this article, experiments were designed and performed to explore the dispersion of solid particles and basic mixing phenomena in compressible free shear layers.

Recent numerical simulations and experiments have shown that the extent of particle dispersion is largely a function of the Stokes number. St is a time scale ratio relating the magnitude of a characteristic τ_f and τ_p:

$$St = \tau_p/\tau_f \tag{1}$$

For a free shear layer, τ_f reflects the motion of the large scale structures, which are known to dominate turbulent shear flows.[8] One simple representation of τ_f is the ratio of the width of the mixing layer (δ, large eddy length scale) and the velocity difference between the two freestreams on either side of the shear layer (large eddy velocity scale). This expression is given by

$$\tau_f = \delta/\Delta U \tag{2}$$

τ_p is the time required for a particle released from rest to accelerate to 63% of a constant freestream velocity, assuming a spherical particle and Stokes drag. The particle response time is given by

$$\tau_p = [d_p^2(\rho_f + 2\rho_p)]/36\mu \tag{3}$$

Note that if $\rho_f << \rho_p$ the equation above reduces to a simpler form given by

$$\tau_p = d_p^2\rho_p/18\mu \tag{4}$$

Recent numerical simulations[9–14] and experimental results[15–18] suggest that there are three ranges of particle response to fluid motion depending on the value of the Stokes number. For Stokes numbers much less than unity (category 1), the particles respond to changes in the flow and thus closely follow the fluid motion. For Stokes numbers much greater than one (category 3), the particles are nearly unaffected by changes in the flow and disperse much less than the fluid. In the broad classification of particle dispersion, characterized by Stokes numbers on the order of unity (category 2), the particles seem to become entrapped in the vortices (large scale structures) and flung outward by a centrifugal force. This centrifuging effect results in particles dispersing more than the carrier fluid. This phenomenon has been observed in both experiments and simulations for incompressible cases and simulations in compressible cases. Past experimental and theo-

Received Aug. 8, 1991; presented as Paper 92-0176 at the AIAA 30th Aerospace Sciences Meeting & Exhibit, Reno, NV, Jan. 6–9, 1992; revision received May 15, 1992; accepted for publication June 12, 1992.

*Graduate Student, ONR Fellow, Department of Mechanical Engineering.
†Associate Professor, Department of Mechanical Engineering. Senior Member AIAA.

retical work both seem to suggest that this ratio of particle to fluid time scales is a major governing nondimensional parameter in particle dispersion in turbulent shear flows. However, the exact range of Stokes number for the three categories discussed above depends on the definition of τ_f from one investigator to another.

Experimental Apparatus and Methods

The experiments were conducted at the Ohio State University Aeronautical and Astronautical Research Laboratory (AARL). The high Reynolds number supersonic blowdown tunnel is a dual-stream tunnel with a 152.4 × 152.4 mm test section. The upper stream is always supersonic while the bottom stream maintains a subsonic flow to match the pressures of the two streams at the tip of the splitter plate, which is needed to maintain a straight, constant pressure shear layer in the test section (Fig. 1). Previous wall pressure measurements (explicitly) and schlieren photographs (implicitly) have shown that static pressure remains constant within the entire test section. Relevant schlieren photographs will be shown and discussed later. The high pressure air is introduced into a settling chamber through a pipe with radial holes. At AARL, cold and dry air is generated at 16.4 MPa (2400 psi) by two four-stage compressors and stored in two storage tanks with 42.5 m^3 (1500 ft^3) capacity.

The top nozzle block is supersonic and interchangeable between nominal Mach 2 and 3 nozzles. The bottom nozzle block is a converging nozzle. A steel splitter plate separates the two flows upstream of the test section (Fig. 1b). Flow parameters for the incoming streams are listed in Table 1. The splitter plate is 3.175-mm thick with a machined angle on the subsonic side of approximately 1 deg over a 125-mm length and a flat profile on the supersonic side. The trailing edge of the splitter plate is machined to a thickness of about 0.5 mm.

Optical access to the test section is provided through the combination of an interchangeable glass window and an access panel on the side walls and glass windows on the top and bottom walls of the tunnel. Interchanging the window and access panel creates a viewing area approximately 80-mm high and 500-mm long. This area includes a 20-mm long view of the incoming boundary layer.

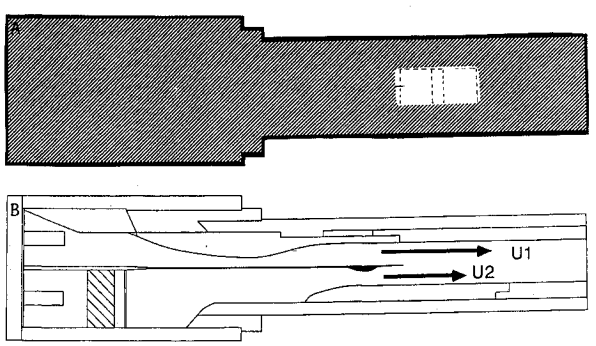

Fig. 1 Schematic of wind tunnel a) view areas and b) cross-sectional view.

Table 1 Flow parameters for the incoming streams

Flow parameter	Case 1	Case 2
U_1, m/s	492	597
U_2, m/s	177	150
M_1	1.83	3.01
M_2	0.51	0.45
ρ_2/ρ_1	0.64	0.37
θ_1, mm	0.62	0.37
$Re_{\theta 1}$	27,700	24,700
Theoretical U_c, m/s	352	428
M_c	0.51	0.86

Changing either of the time scales τ_p or τ_f will change St and ultimately the particle dispersion [Eq. (1)]. In this experiment, the particle size alone is changed to vary τ_p and two different flow conditions are used to vary τ_f. These combinations compose six different time scale ratios.

To assure consistent drag force as calculated by Stokes drag law, the particles need to be spherical and uniform in both size and density. Spherical glass beads from Potters Industries Inc. were the most economical material for our purposes. The particles purchased from this company were sorted (air classified) by the Vortec Products Company to obtain particle groups with nominal diameters of 5, 17, and 62 μm, all with a nominal diameter tolerance of ± 2 μm (Fig. 2). A 100-μm scale is shown in this figure.

A two-phase flow of spherical particles suspended in air is pumped through two tubes passing through opposite sides of the tunnel sidewalls and into channels in an injection wedge mounted on the subsonic side of the splitter plate. The wedge was made from a 1.27 × 152 × 152 mm aluminum plate. The thickness of the trailing and the leading edges of the wedge was approximately 0.5 mm. This was obtained by machining the 1.27-mm-thick plate with an approximately 10-deg slope toward the leading and trailing edges to minimize flow disturbances or modifications of incoming nozzle flow. Since the particle injection wedge was located in the subsonic side which is driven by the supersonic flow (similar to a supersonic-subsonic ejector system), the wedge's effect on the base flow was expected to be very small. Figures 3 and 4 are long-exposure ($\approx$1 ms) schlieren photographs of the flowfield without and with the particle injection wedge mounted for cases 1 and 2. Each photograph has two segments; one segment for the upstream and one for the downstream region of the mixing layer. There is an overlap in case 1 and a gap in case 2 due to the physical restrains in the tunnel. The dark line on all the photographs indicates the physical $y = 0$ (x coordinate) location. This line was drawn on the schlieren image plane. As was expected, these and also short exposure (0.5 μs) images (not reported here) did not show any observable effect of the injection wedge in the flowfields. Also, since the shear

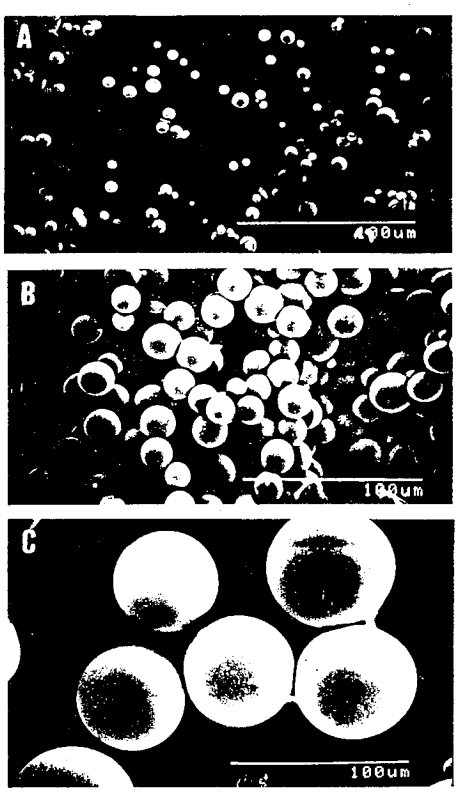

Fig. 2 SEM photographs of particle groups: a) group a, b) group b, and c) group c.

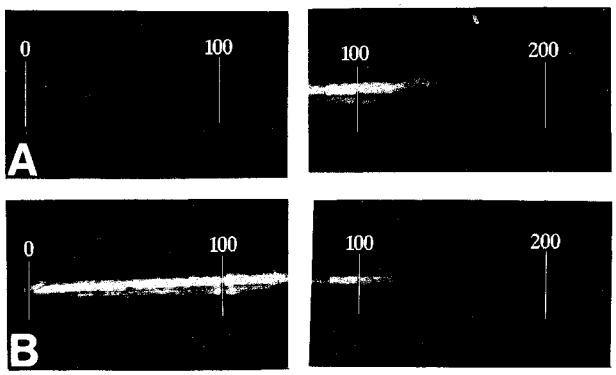

Fig. 3 Schlieren images for M_c = 0.51 a) without wedge and b) with wedge; the dark horizontal line is level with the splitter plate; units in mm.

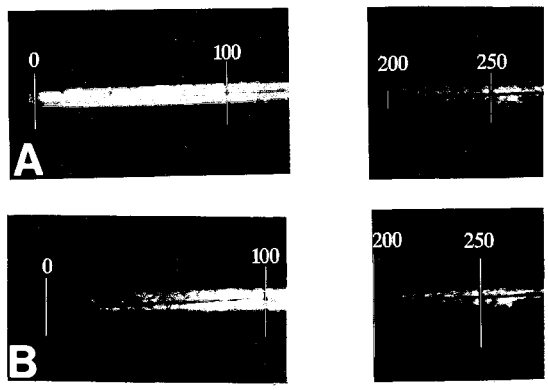

Fig. 4 Schlieren images for M_c = 0.86 a) without wedge and b) with wedge; the dark horizontal line is level with the splitter plate; units in mm.

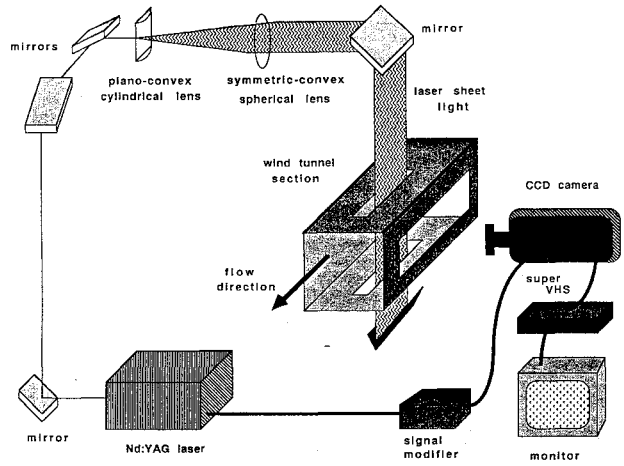

Fig. 5 Laser sheet lighting and image recording system.

layer is not deflected toward either the supersonic or subsonic flow, these photographs confirm that pressure in the test section was constant with and without the particle injection system. The injection of particles is made, in the streamwise direction, through a series of holes on the rear-facing slope of the wedge at a station 14.6-cm upstream of the trailing edge of the splitter plate (Fig. 1b). A MARK XII fine powder feeder was used to supply a reasonably constant, low mass flow of glass beads to the injection wedge. The powder feeder consists of a pressurized, sealed powder canister, a variable speed screw assembly, and a carburetor.

A Quanta-Ray GCR-4 Pulsed Nd:YAG laser manufactured by Spectra Physics was used in this experiment. The laser, operated without amplification (oscillator only), produced approximately 250 mJ/pulse of energy. The pulsed laser has a wavelength of 532 nm, a pulse width of approximately 9 ns, and a repetition rate of 10 Hz. Mirrors and lenses were used to form a sheet of laser light approximately 14.5-mm wide and calculated to be a fraction of a mm thick. The laser sheet was oriented to illuminate glass beads in a streamwise slice of the shear layer, parallel to the wind-tunnel's side walls. Figure 5 illustrates the laser sheet lighting and image recording system.

A double-intensified gated CCD camera, focused on the vertical sheet of laser light passed through the wind tunnel, recorded instantaneous images on a super VHS tape. The images on the tape were later transferred to a computer using a frame grabber. The resulting raw data was the intensity (on a scale of 0–255) of each pixel in a 480 × 512 grid configuration which was stored on a MASSCOMP 5520 computer and subsequently used for image processing.

Digital Image Processing

Flow visualization and subsequent analysis of digitized images were used to locate the particles' positions for statistical analysis. Approximately 150 images were selected and digitized from each of the six flow conditions. The selection criteria were 1) the image to contain enough particles to contribute to the statistical calculations (minimum of about 20 particles), and 2) the image not to be dominated by clumping and visually overlapping particles characteristic of a surge in the particle injection system. The criterion 2) was used to eliminate data resulting from sporadic high particle loading in which particles could possibly influence the base flow.

The laser beam was expanded into a sheet and brought into the tunnel from the top window (Fig. 5). The Gaussian nature of the laser sheet light caused a nonuniform trend in the x direction of the image. Note that the flow is in the x direction relative to the coordinate system of the images. The average intensity values of the center column pixels were larger than the average intensity values of the edge column pixels. This prohibited the use of a global threshold intensity value to distinguish between particle and background intensities on the original images. This problem was circumvented by computing local thresholds that vary along the direction of the nonuniformity.[19] The program identified particle images by examining group patterns of adjacent pixels brighter than their corresponding threshold intensities. The size and intensity of the bright pixel groups representing the particles depend jointly on particle light scattering characteristics, particle motion, illuminating properties, and recording device properties. The average size and intensity of the particle image were obtained statistically. Average and standard deviation values for particle image size and particle image average intensity were used to identify and eliminate data generated by means other than a single particle passing through the laser sheet. The total number of particles included in the calculations for Figs. 6–14 ranged from 3537 to 8653 particles depending on the case.

After verifying that the particle images were the result of light scattered from one of the glass beads passing through

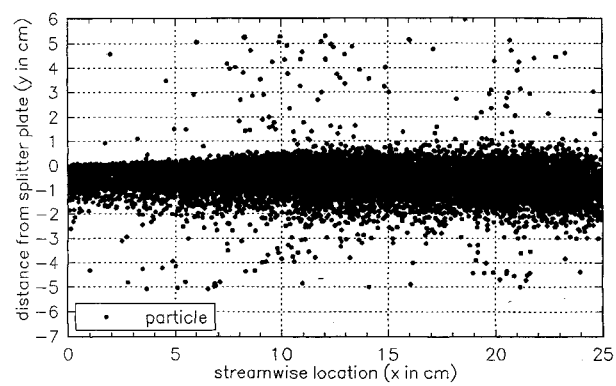

Fig. 6 Particle locations for case 1a: M_c = 0.51, particle size = 1–8 μm, St_δ = 7.

the laser sheet, the data were scaled and rotated. This enabled direct physical comparison between all the test runs since each image was represented on the same scale and orientation. The physical reference points were produced by passing light through a series of pinholes in the black masking on the far wall of the wind tunnel.

Results and Discussion

Long-exposure schlieren images of the $M_c = 0.51$ and $M_c = 0.86$ free shear layers show that matching the static pressures of the top and bottom streams maintains a straight shear layer with respect to the splitter plate and the top and bottom walls bounding the flow (see Figs. 3 and 4). Previous studies have shown that the structures in the $M_c = 0.51$ case are similar to incompressible mixing layers, relatively well organized, and two-dimensional to a large degree with relatively well defined core and braid regions.[20,21] However, in the $M_c = 0.86$ free shear layer the structures are much less organized and more three-dimensional, and the mixing layer is characterized by substantially reduced growth rate and turbulent momentum exchange relative to the $M_c = 0.51$ case.[7,20,21]

Long-time-exposure photographs of particle-laden mixing layers would reveal general trends in dispersion of particles. In the present experiment, long time-exposure photograph-like images were obtained by superimposing many digital images. Figures 6–8 and 10–12 each show the superposition of particle locations from over 300 images. Two adjacent viewing areas were necessary to cover the total 25-cm streamwise segment of the mixing layer shown in the figures. Approximately 150 images were used from each the upstream ($x = -1.0$ to $+15.0$ cm) and the downstream ($x = 10.0$ to 26.0 cm) viewing areas for these superimposed images. The final plots therefore include an overlapping area in the range from approximately $x = 10.0$–15.0 cm (Fig. 1a). The origin of these plots ($x, y = 0, 0$) represents the trailing edge of the splitter plate. The dark solid line on the schlieren images (Figs. 3 and 4) indicates the physical x-coordinate location. The solid circles used to mark the particle locations on the figures are the same size for all cases. The solid circles do not reflect the true particle size or the recorded particle image size. It should be mentioned that the mass loadings of particles (the ratio of particle mass flow to carrier gas mass flow) was very small. As was mentioned earlier, each image was examined and any image with clustered particles was eliminated to maintain the very low particle loading data. Previous researchers have concluded that with such a small particle loading the effect of particles on the base flow is essentially negligible.[11]

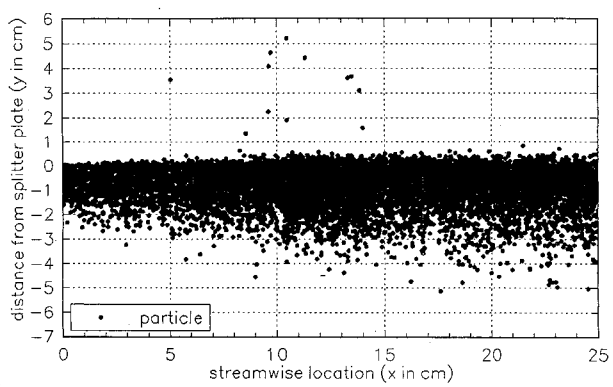

Fig. 7 Particle locations for case 1b: $M_c = 0.51$, particle size = 15–20 μm, $St_\delta = 84$.

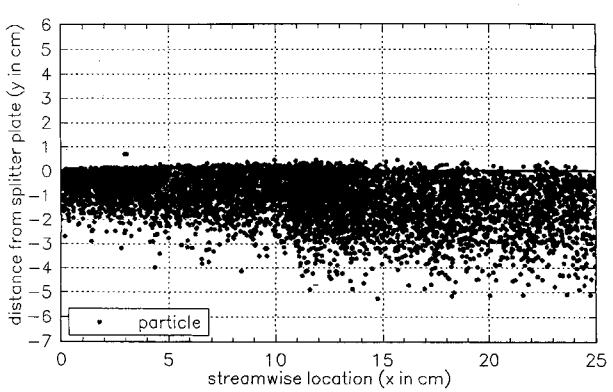

Fig. 8 Particle locations for case 1c: $M_c = 0.51$, particle size = 60–65 μm, $St_\delta = 1116$.

Figures 6–8 all represent the flowfield in case 1, $M_c = 0.51$, with three different particle groups; groups a, b, and c. These three cases, therefore, will be called cases 1a, 1b, and 1c, respectively. Table 2 lists the particle diameter range and the dimensional St for these cases. In this table, St_δ ($St_\delta = St \times \delta$) is listed rather than St. The flow length scale is changing substantially in the streamwise direction. If one takes the flow length scale to be the mixing layer thickness, the length scale changes from a very small value at $x = 0$ cm to approximately 2 cm at $x = 22$ cm. Thus, for case 1a the Stokes number changes from a very large value close to the splitter plate to approximately 3.5 further downstream in the mixing layer.

Since the flow length scale is the same for cases 1a–c ($M_c = 0.51$), the differences in the results for these three cases can be directly attributed to Stokes number differences. If the flow length scale is taken to be 1 cm, which corresponds to the mixing layer thickness at approximately $x = 10$ cm, the Stokes number changes from 7 for case 1a (Fig. 6) to 1116 for case 1c (Fig. 8). It should be mentioned that the wider size distribution (larger standard deviation of the particle diameters) of particle group a relative to groups b and c may slightly mask the results. Many particles in case 1a and some in case 1b are thrown deep into the supersonic freestream. The likely mechanism for this observation is that these particles were entrained into large scale structures and subsequently thrown out of the mixing layer due to centrifugal forces. As mentioned previously, several studies have highlighted this type of selective dispersion on the basis of Stokes number. These studies seem to suggest that particles will be ousted from the mixing layer for Stokes numbers on the order of 1. The disperison for case 1a shown in Fig. 6 (for which the representative Stokes number is calculated to be 7) seems to agree with the theoretical predictions. Furthermore, cases 1a–c in Figs. 6–8 seem to follow the expected trend from Stokes number arguments.[9–18] Namely, the particles charac-

Table 2 Dimensional Stokes numbers

Dimensional Stokes number for $M_c = 0.51$				
	Size	d_p, μm	τ_p, s	St_δ, cm
Case 1a	min	1	0.0001	0.3
	avg	5	0.0002	7
	max	7	0.0006	19
Case 1b	min	15	0.0021	65
	avg	17	0.0027	84
	max	20	0.0037	116
Case 1c	min	60	0.0332	1045
	avg	62	0.0354	1116
	max	65	0.0389	1226
Dimensional Stokes number for $M_c = 0.86$				
	Size	d_p, μm	τ_p, s	St_δ, cm
Case 2a	min	1	0.0001	0.5
	avg	5	0.0003	12
	max	7	0.0007	30
Case 2b	min	15	0.0024	106
	avg	17	0.0031	136
	max	20	0.0042	189
Case 2c	min	60	0.0380	1700
	avg	62	0.0406	1815
	max	65	0.0446	1995

Particle material = solid glass. Particle material density = 2.5 g/cm^3.

terized by higher Stokes numbers spread less into the high speed side of the shear layer. Figure 9 shows the boundaries within which 90% of the particles for each of the three cases reside (i.e., 5% of the particle population is above and 5% is below these boundaries at each streamwise location). These boundary curves are not smooth because of the limited number of samples. The previously cited trend of decreased dispersion with increasing Stokes number is quite clear. Case 1a on the average has penetrated more into the high speed stream than case 1b, and case 1b has penetrated much more than case 1c.

Instead of being totally unaffected by fluid motion, the particles of largest Stokes number appear to be affected to some extent by the diverging configuration of the shear layer. It is well documented that as one moves downstream in a mixing layer composed of one supersonic and one subsonic stream, lines of constant velocity diverge farther from the center of the mixing layer in the subsonic side than the supersonic side.[22,23] For example, Ikawa[22] showed the lower-most constant lines of the mixing layer to be at a diverging angle approximately four times the uppermost ones. The schlieren photographs shown in Figs. 3 and 4 do not indicate this phenomenon due to the weak density gradient in the subsonic side. This misleading schlieren phenomenon can be seen in Figs. 3 and 4 where the incoming boundary layer for the high speed side is clearly shown but the boundary layer on the subsonic side is not visible. It appears that the downstream evolution of the average particle location is representative of this diverging shear layer structure at high Stokes numbers (cases 1b and 1c). As expected, the downstream evolution of the 90% envelope of the particles with lower Stokes numbers (case 1a) does not show this trend. This could be because the dispersion due to large scale flow structures is a much more prominent effect at low Stokes numbers than is the diverging mean flow.

Figures 10–12 show the superimposed images for cases 2a–c. The flow in these cases is $M_c = 0.86$ and the particles for

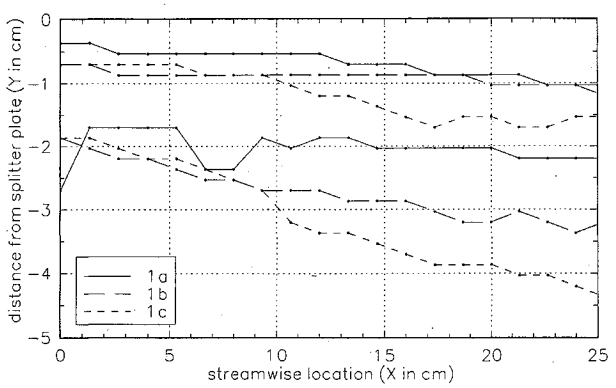

Fig. 9 90% Population boundaries for $M_c = 0.51$.

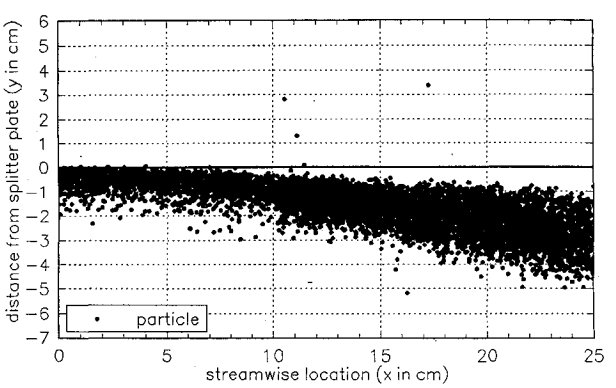

Fig. 10 Particle locations for case 2a: $M_c = 0.86$, particle size = 1–8 μm, $St_\delta = 12$.

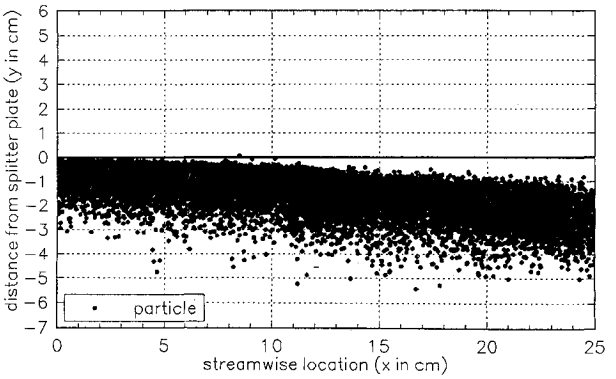

Fig. 11 Particle locations for case 2b: $M_c = 0.86$, particle size = 15–20 μm, $St_\delta = 136$.

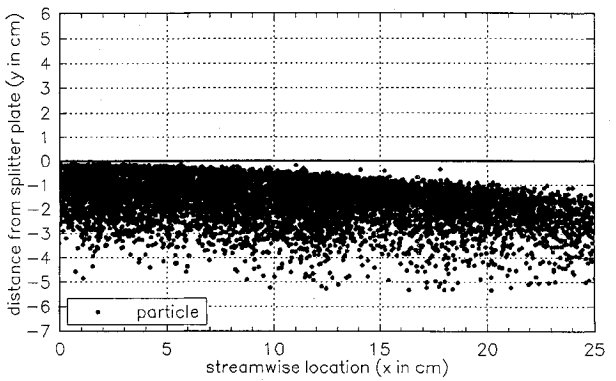

Fig. 12 Particle locations for case 2c: $M_c = 0.86$, particle size = 60–65 μm, $St_\delta = 1995$.

cases a–c are from the same groups as in Figs. 6–8, respectively. Neglecting the very few particles that were ejected into the supersonic freestream in case 2a, one does not see any observable Stokes number effects in these figures as far as the penetration of particles into the supersonic stream is concerned. The striking feature of these results is that the mixing region marked by these particles has been substantially skewed (or bent) toward the low-speed side of the mixing region. As previously discussed, this is a constant pressure mixing layer and schlieren photographs shown in Fig. 4 clearly show that the mixing layer is straight.

A possible explanation for the particle dispersion's apparent independence of Stokes number in cases 2a–c can be formulated if one considers more closely the flow time scale. Recent work indicates that the large-scale flow structures in the mixing layer of case 2 ($M_c = 0.86$) are much less organized than in case 1 ($M_c = 0.51$) and appear to be more three-dimensional and oblique in the spanwise direction.[20,21] Consequently, the flow length scale becomes significantly smaller in case 2 causing the Stokes number to increase, possibly resulting in case 2a (and subsequently 2b and 2c) belonging to the broad category of particles of sufficiently high Stokes numbers such that their dispersion is not affected by fluctuations in the fluid motion. Samimy and Lele's[13,14] results for M_c values up to 0.6 did not show any compressibility effects. However, their recent results (work in progress) show a significant compressibility effect for the $Mc = 0.86$ case.

Figure 13 shows the boundaries within which 90% of the particles reside for cases 2a–c. It appears that none of the particle groups in case 2 are noticeably dispersed by the large scale fluid structures. Instead, their trajectories are reminiscent of the divergent configuration of the shear layer previously mentioned. This trend is similar to that seen in case 1c. One might think that the trend seen in Figs. 10–12 is caused by the force of gravity. However, calculations show that the downward trajectory of the particles represented in Fig. 13 cannot solely be an affect of gravity.[19]

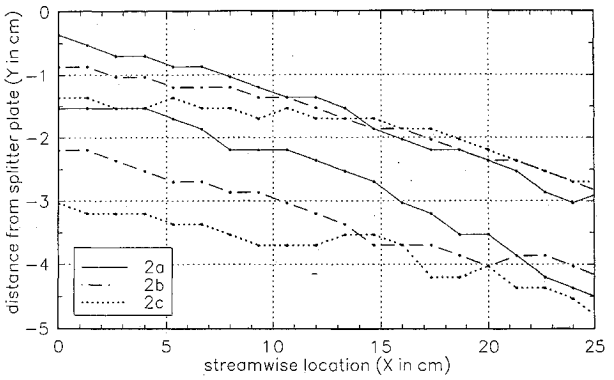

Fig. 13 90% Population boundaries for $M_c = 0.86$.

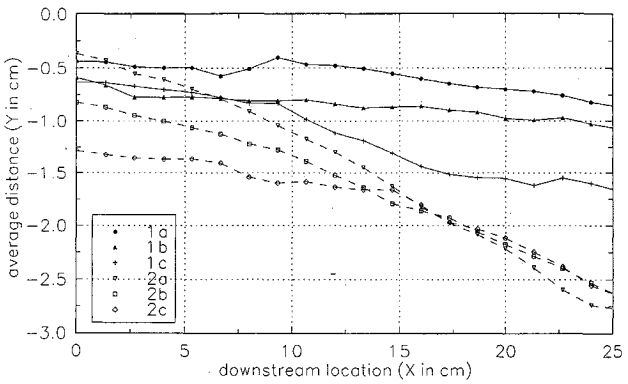

Fig. 14 Particle average location relative to splitter plate.

Figure 14 shows the average particle location for all the six cases shown in Figs. 6–8 and Figs. 10–12. The trend in cases 1a–c is quite clear. From this figure it is also clear that the same vertical particle location at the tip of the splitter plate ($x = 0$ cm) is not achieved for all of the cases. Ideally, the particles achieve the subsonic freestream velocity by the time they reach the tip of the splitter plate and are introduced into the mixing layer at the same location. However, achieved experimental conditions are far from ideal. The particle velocity is unknown and the average particle y location at the splitter plate tip ($x = 0$ cm) decreases as the particle size increases, especially for case 2. Based on a simple calculation, this is not entirely an effect of gravity.[19] The calculated vertical displacement due to gravity by the time the particle reaches the end of the splitter plate ($x = 0$ cm) is only $y = -0.196$ cm for the largest particles. The most probable cause of this displacement is the interaction of the particles with the boundary layer on the bottom side of the splitter plate.

The fact that the vertical particle elevation at the tip of the splitter plate decrease with increasing particle size may be a cause for reduced dispersion. However, recent spatially evolving numerical simulations by Samimy and Lele (work in progress) seem to indicate that regardless of the initial particle release location, the particles with similar Stokes numbers get entrained into the mixing layer and eventually follow similar paths. This phenomenon is particularly evident in case 2 where all cases 2a–c have such high Stokes numbers (far into category 3). Figure 14 shows the average particle location for cases 2a–c to be initially different. However, this difference vanishes further downstream as the particles average location for the three cases converges for $x > 15$ cm. Cases 1a–c do not show this phenomenon since their smaller Stokes numbers fall in different categories; thus making them behave differently.

In these experiments we do not have any particles with a small enough Stokes number to accurately follow the flow (category 1). Case 1a seems to fall into the category of particles with medium Stokes numbers which are significantly affected by large scale structures (category 2). Cases 1c and 2a–c seem to fall into the category of particles with large Stokes numbers which are not significantly affected by large scale structures and disperse much less than fluid elements (category 3). The particles in case 1b seem to be on the borderline of the latter two categories.

One might expect case 2a to be in category 2 or on the borderline of categories 2 and 3 because St_δ for case 2a is comparable to St_δ for case 1a. However, this does not appear to be the case. A probable explanation is the previously discussed differences in the large-scale flow structures of cases 1 and 2. As discussed previously, this results in an increased Stokes number pushing the particles of case 2 into category 3.

In case 1a (Fig. 6), the majority of isolated particles appear to reside near the central region of the view areas ($x = 8$–13 cm) and ($x = 19$–22 cm). While one could conclude that these are the result of selective dispersion due to some nearly stationary vortices at these streamwise locations, it is more probable that this is an effect of the Gaussian attribute of the illuminating laser sheet light. The Gaussian attribute causes the intensity of the laser sheet light to be most intense at the center and decrease toward the edges. Particles passing through the edges of the sheet are illuminated by less intense light. The resulting light intensity scattered by the particles may be so low that it is not distinguished from the background intensity by either the CCD camera or the subsequent image processing. Therefore, the number of validated samples is significantly larger for the central region of the viewing areas. The apparent low particle population from $x = 0$ to 8 cm and $x = 14$ to 19 cm are most likely not a true particle dispersion effect.

Barring unknown variables in the illuminating and recording devices, these plots are an overall indication of the dispersion occurring in these experiments. A recommendation to avoid problems caused by the Gaussian attribute of the laser beam is to use more viewing areas each overlapping the other by roughly one-half the width of the laser sheet. This will assure that each location in the flowfield has been illuminated by at least one intense area of the incident laser sheet light. Superimposing these overlapping view areas in their relative positions should result in a more consistent image.

Conclusion

Previous investigators have shown that for incompressible flow, particle response can be divided into three categories based on the Stokes number which includes both flow and particle parameters. Particles with small Stokes numbers follow the flow and disperse as much as the fluid elements (category 1), particles of very large Stokes numbers are not appreciably affected by large scale structures and disperse much less (category 3), and particles of intermediate Stokes numbers disperse much more than the fluid elements (category 2). In the present experiments, two mixing layers [one borderline compressible-incompressible ($M_c = 0.51$) and one highly compressible ($M_c = 0.86$)] together with three sets of particles were used to investigate compressibility effects on particle dispersion. None of the six resulting combinations created a Stokes number small enough for the particles to follow the flow (category 1). The results for the low compressibility case ($M_c = 0.51$) show trends very similar to incompressible flow cases in the category 2 and 3 range. However, the results for the high compressibility case ($M_c = 0.86$) show the particles to be unaffected (category 3 only) by the poorly organized and highly three-dimensional large-scale structures resulting from the higher compressibility. It seems the large structures in the higher compressibility case cannot entrain and disperse the particles as effectively as the more two-dimensional, more organized structures of low compressibility and incompressible mixing layers. The probability that the less organized flow structures in the higher compressibility case cause a smaller fluid time scale (consequently causing St to take on a very

high value) is offered as a means of explaining the observed trends in the context of Stokes number-dependent particle dispersion. Furthermore, these experiments show that injecting solid fuel particles in highly compressible mixing layers of applications such as scramjets would not result in enhanced mixing.

Acknowledgments

This work was supported by the Office of Naval Research under Contract N00014-90-J-1730 (with S. G. Lekoudis and P. Purtell as the Technical Monitors) and by the ONR Fellowship Program.

References

[1]Kumar, A., Bushnell, D. M., and Hussaini, M. Y., "A Mixing Augmentation Technique for Hypervelocity Scramjets," AIAA/SAE/ASME/ASEE 23rd Joint Propulsion Conf., AIAA Paper 87-1882, San Diego, CA, June 1987.

[2]Waltrup, P. J., "Liquid-Fueled Supersonic Combustion Ramjets: A Research Perspective," *Journal of Propulsion*, Vol. 3, No. 6, 1987, pp. 515–524.

[3]Snyder, T. S., Jarymowycz, T. A., Pace, K. K., and Kuo, K. K., "Solid Fuel Ignition and Combustion Characteristics Under High-Speed Crossflows," AIAA/SAE/ASME/ASEE 26th Joint Propulsion Conf., AIAA Paper 90-2075, Orlando, FL, July 1990.

[4]Bogdanoff, D. W., "Compressibility Effects in Turbulent Shear Layers," *AIAA Journal*, Vol. 21, No. 6, 1983, pp. 926–927.

[5]Papamoschou, D., and Roshko, A., "The Compressible Turbulent Mixing Layer: An Experimental Study," *Journal of Fluid Mechanics*, Vol. 197, 1988, pp. 453–477.

[6]Samimy, M., and Elliott, G. S., "Effects of Compressibility on the Characteristics of Free Shear Layers," *AIAA Journal*, Vol. 28, No. 3, 1990, pp. 439–445.

[7]Elliott, G. S., and Samimy, M., "Compressibility Effects in Free Shear Layers," *Physics of Fluids A*, Vol. 2, No. 7, 1990, pp. 1231–1240.

[8]Brown, G. L., and Roshko, A., "On Density Effects and Large Scale Structures in Turbulent Mixing Layers," *Journal of Fluid Mechanics*, Vol. 64, 1974, pp. 75–816.

[9]Chein, R., and Chung, J. N., "Simulation of Particle Dispersion in a Two-Dimensional Mixing Layer," *AIChE Journal*, Vol. 36, No. 6, 1988, pp. 946–954.

[10]Chung, J. N., and Troutt, T. R., "Simulation of Particle Dispersion in an Axisymmetric Jet," *Journal of Fluid Mechanics*, Vol. 186, 1988, pp. 199–222.

[11]Crowe, C. T., Chung, J. N., and Troutt, T. R., "Particle Mixing in Free Shear Flows," *Progress in Energy and Combustion Science*, Vol. 14, 1988, pp. 171–194.

[12]Crowe, C. T., Gore, R. A., and Troutt, T. R., "Particle Dispersion by Coherent Structures in Free Shear Flows," *Particulate Science and Technology*, Vol. 3, 1985, pp. 149–158.

[13]Samimy, M., and Lele, S. K., "Particle-Laden Compressible Free Shear Layers," AIAA/SAE/ASME/ASEE 26th Joint Propulsion Conf., AIAA Paper 90-1977, Orlando, FL, July 1990.

[14]Samimy, M., and Lele, S. K., "Motion of Particles with Inertia in a Compressible Free Shear Layer," *Physics of Fluid A*, Vol. 3, No. 8, 1991, pp. 1915–1923.

[15]Kamalu, N., Wen, F., Troutt, T. R., Crowe, C. T., and Chung, J. N., "Particle Dispersion by Ordered Motion in Turbulent Mixing Layers," *ASME Forum on Cavitation and Multiphase Flow*, July 1988, pp. 150–154.

[16]Kamalu, N., Tang, L., Troutt, T. R., Chung, J. N., and Crowe, C. T., "Particle Dispersion in Developing Shear Layers," *International Conference on Mechanics of Two-Phase Flows*, Taipei, Taiwan, June 1989, pp. 199–202.

[17]Lázaro, B. J., and Lasheras, J. C., "Particle Dispersion in a Turbulent, Plane, Free Shear Layer," *Physics of Fluids A*, Vol. 1, No. 6, 1989, pp. 1035–1044.

[18]Longmire, E. K., "Structure and Control of a Particle-Laden Jet," Ph.D. Dissertation, Stanford Univ., Stanford, CA, 1990.

[19]Glawe, D. D., "Dispersion of Large Particles in Compressible Free Shear Layers," M.S. Thesis, Ohio State Univ., Columbus, OH, 1991.

[20]Samimy, M., Reeder, M. F., and Elliott, G. S. "Compressibility Effects on Large Structures in Free Shear Flows," *Physics of Fluids A*, Vol. 4, No. 6, 1992, pp. 1251–1258.

[21]Elliott, G. S., Samimy, M., and Arnette, S. A., "A Study of Compressible Mixing Layers Using Filtered Rayleigh Scattering Based Visualizations," *AIAA Journal* (to be published).

[22]Ikawa, H., "Turbulent Mixing Layer Experiment in Supersonic Flow," Ph.D. Dissertation, California Inst. of Technology, Pasadena, CA, 1973.

[23]Petrie, H. L., "A Study of Compressible Turbulent Free Shear Layers Using Laser Doppler Velocimetry," Ph.D. Dissertation, Univ. of Illinois, Urbana, IL, 1984.